Heliyon 9 (2023) e13212

Contents lists available at ScienceDirect

Heliyon

journal homepage: www.cell.com/heliyon

Research article

# Modelling, mapping and monitoring of forest cover changes, using support vector machine, kernel logistic regression and naive bayes tree models with optical remote sensing data

Aqil Tariq [a], Yan Jiango [a,*], Qingting Li [b], Jianwei Gao [c], Linlin Lu [d,**], Walid Soufan [e], Khalid F. Almutairi [e], Muhammad Habib-ur-Rahman [f]

[a] State Key Laboratory of Information Engineering in Surveying, Mapping and Remote Sensing, Wuhan University, Wuhan, 430079, Hubei, China
[b] Airborne Remote Sensing Center, Aerospace Information Research Institute, Chinese Academy of Sciences, Beijing 100094, China
[c] Institute of Spacecraft Application System Engineering, China Academy of Space Technology, Beijing, 100094, China
[d] Key Laboratory of Digital Earth Science, Aerospace Information Research Institute, Chinese Academy of Sciences, Beijing 100094, China
[e] Plant Production Department, College of Food and Agriculture Sciences, King Saud University, P.O. Box 2460, Riyadh 11451, Saudi Arabia
[f] Institute of Crop Science and Resource Conservation (INRES), Crop Science, University of Bonn, 53115, Bonn, Germany

ARTICLE INFO

*Keywords:*
Forest cover
Naive bayes tree
Kernel logistic regression
Support vector machine
Change detection
Landsat

ABSTRACT

The present study is designed to monitor the spatio-temporal changes in forest cover using Remote Sensing (RS) and Geographic Information system (GIS) techniques from 1990 to 2017. Landsat data from 1990 (Thematic mapper [TM]), 2000 and 2010 (Enhanced Thematic Mapper [ETM+]), and 2013 to 2017 (Operational Land Imager/Thermal Infrared Sensor [OLI/TIRS]) were classified into the classes termed snow, water, barren land, built-up area, forest, and vegetation. The method was built using multitemporal Landsat images and the machine learning techniques Support Vector Machine (SVM), Naive Bayes Tree (NBT) and Kernel Logistic Regression (KLR). According to the results, forest area was decreased from 19,360 $km^2$ (26.0%) to 18,784 $km^2$ (25.2%) from 1990 to 2010, while forest area was increased from 18,640 $km^2$ (25.0%) to 26,765 $km^2$ (35.9%) area from 2013 to 2017 due to "One billion tree Project". According to our findings, SVM performed better than KLR and NBT on all three accuracy metrics (recall, precision, and accuracy) and the F1 score was >0.89. The study demonstrated that concurrent reforestation in barren land areas improved methods of sustaining the forest and RS and GIS into everyday forestry organization practices in Khyber Pakhtun Khwa (KPK), Pakistan. The study results were beneficial, especially at the decision-making level for the local or provincial government of KPK and for understanding the global scenario for regional planning.

## 1. Introduction

Forest transformation is defined as the changes occurring in a country's forest cover from a period of contraction to a period of expansion. A forest change includes patterns from growing forest areas over time [1–3]. From a social and economic point of view,

*Abbreviations:* LULC, Landuse land cover; SVM, Support Vector Machine; KLR, Kernel Logistic Regression; NBT, Naive Bayes Tree.

* Corresponding author.
** Corresponding author.
*E-mail addresses:* aqiltariq@whu.edu.cn (A. Tariq), Jgyan@whu.edu.cn (Y. Jiango), lull@radi.ac.cn (L. Lu).

https://doi.org/10.1016/j.heliyon.2023.e13212
Received 9 April 2022; Received in revised form 16 January 2023; Accepted 19 January 2023
Available online 26 January 2023

forests are a source of firewood and timber for construction which play an essential role in sustaining atmospheric carbon (anthropological and natural emissions) and thus contributing to mitigating the climate change [4–7]. The rapid loss of forests contributes to global climate change [8]. Logging, forestry, mining, and other human activities have changed about six million hectares (MHA) of forest worldwide [9]. According to the United Nations Framework Convention on Climate Change (UNFCCC), agriculture is the leading cause of deforestation. Commercial agriculture accounts for 32%; current agriculture accounts for 48%; forest use (infrastructure expansion such as road building and urbanization) accounts for 14%, and timber harvesting accounts for 5% of deforestation [10–12]. From an ecological point of view, forests avoid the loss of the top layers of fertile soil, which explains their importance for the entire ecosystem. The damaged canal can be visualized in deforested areas, where poor soils have significantly reduced agricultural production and hinder the potential for subsequent reforestation [6,13–16].

The forest area of Pakistan is almost 4.8 MHA in all its topographical areas [17], covering 1.98 MHA of coniferous hill forests; 1.81 MHA of foothill forests; 0.229 MHA of irrigated crops, 0.280 MHA of the river and 0.35 MHA of mangroves in the Indus River delta [18]. Pakistan's forest reservoirs are mainly located in the northern regions (6.5% in Azad Kashmir, 15.7% in Gilgit Baltistan, and 40% in Khyber Pakhtun khawa (KPK)). Forests are mainly scattered in the Karakoram, Hindukush, and Himalayan mountains and scrub in KPK. Coniferous forests are primarily located on the upper slopes of the Manshera, Mardan, Sawat, Upper Dir, Lower Dir, and Chitral Districts, where alpine pastures are rare [9].

Governments need innovative reforestation policies and programs to avoid high deforestation rates and encourage the transformation of forests. In addition to Pakistan's KPK area, some countries, such as the Republic of Korea, Vietnam, China, Japan, and the Philippines, have increased their forest cover or suffered forest change due to government action through a series of reforestation policies and programs [19–26]. Comparing these government interventions among countries is essential to provide valuable lessons to stop deforestation and improve forest coverage, especially in developing countries. The KPK's productive forest evolution through national forest policies is incredibly privileged and can be implemented in Pakistan and other developing countries to avoid deforestation and enhance their natural environments. The change recognition system assesses Land Use Land Covers (LULC) such as forest or vegetation and flood monitoring [5,27].

In previous studies [28–30], vegetation indices are considered a good indicator of the changes in the area surrounded by vegetation. To recognize the spatio-temporal evolution of vegetation indices in a semi-arid region and the relationship with the urbanization phenomenon, multi-temporal satellite image data such as MSS and ETM + have been employed previously to identify this shift using four vegetation indices (namely Transformed Soil Adjusted Vegetation Index (TSAVI), Soil Adjusted Vegetation Index (SAVI), Normalize Vegetation Difference Index (NDVI), and Transformed Vegetation Index (TVI)). The SAVI index is used to mitigate the effects of soil reflection [31]. The SAVI design is also suitable for low vegetation cover, especially in semi-arid regions. As a result, these indices could not always identify the difference between vegetation and non-vegetation regions [32]. Classification techniques can be divided into the following five groups: (a) advanced classification, (b) supervised classification; (c); unsupervised classification; (d) Object-Based Image Analysis (OBIA); and (e) sub-pixel classification. For LULC classification and mapping, numerous ML methods have been developed recently. LULC classification and forest mapping using Landsat images make extensive use of ensemble ML methods like Random Forest (RF) [33], prediction of LULC [14], forest change forecasting, and land use planning [27].

Previous researchers integrated image processing with supervised classification for mapping and classifying forest changes. There needs to be more research done locally that makes use of RS data. However, these studies [34,35], only used traditional methods like visual interpretation and traditional classifiers of optical remote sensing images. Sometimes, these methods were combined with manual digitization methods to map the forest cover and non-forest cover areas.

Extensive regional categorization and forest monitoring have been demonstrated by integrating NBT, KLR, SVM, and image differences [36]. Compared to conventional classifiers like maximum likelihood, these methods can lessen the modification and overfitting of the arrangement maps while evaluating several variables independently [37]. Accordingly, we employed the combination of KLR and SVM to extract spatial and temporal information about the KPK forests. By employing ML methods, variation and overfitting in the resulting categorized maps are reduced [35,38–41]. Several factors have aggravated deforestation and land destruction in KPK in 2010. These can be considered direct and indirect factors. The indirect factors of government officials were corruption, poor policies, lack of law enforcement, and poverty. The main factors were population growth, exploitation of fuelwood, unsustainable farming practices, illegal logging, wildland fires, and mining activities [35,15]. The reforestation took place throughout the KPK in 2014 [42]. This program was launched as part of the "One Billion Tree Project" to promote forest areas, enhance biodiversity, and monitor deforestation. A large part of the forest area was changed from 2013 to 2017 [42]. Mapping and monitoring the KPK rainforest with satellite imagery is not easy.

This research aims to monitor the forest cover change by using satellite imagery. Data were collected via Landsat using RS and GIS techniques. The information would deliver primary evidence and ground knowledge for developing a forest cover map for the "Ten Billion field project". Consequently, this study aims to present the machine learning approach that combines SVM with KLR and NBT algorithms and uses of Landsat 5,7 and 8 images for spatio-temporal mapping of the KPK forests, evaluate the performance of these algorithms, and put into practice a change detection strategy to track the evolution of the forest from 1990 to 2017.

## 2. Materials and methods

### 2.1. Study area

The study area selected was Khyber Pakhtun Khwa (KPK) province of Pakistan which is located between latitude 31° 40′ to 36° 57′ N and longitude 69° 19′ to 74° 70′ E in the circle of Hindukush and Himalaya Ranges, which are the world's top mountain ranges

(Fig. 1). The Hindukush range stretches along the western border, while the Himalayas stretches from North to East [43]. Many climate changes in the province were caused by significant changes in physiological characteristics and altitude. Therefore, the southern parts are dry and arid, while the northern parts are cold and humid. The northern mountains form a cold desert of high altitudes. In its central position, the Peshawar Valley has temperate weather. The average annual temperature in the south varies as per different seasons [44].

### 2.2. Remote sensing data and processing

In this study, we used Landsat 5 (TM), 7 (ETM+), and 8 (OLI/TIRS) RS data. We relied on Landsat images since they were freely available, cost nothing, had good spatio-temporal and spectral resolutions, and came in handy time series [18]. In addition, Landsat images with less cloud cover are given in orthorectification format [45]. Landsat 5, 7, and 8 images with 30 m spatial and 16 days temporal resolution were used [46]. Digital Elevation Model data (DEMs; 30 $m \times 30$ $m$) provided by the NASA Shuttle Radar Topographic Mission (SRTM, http://srtm.csi.cgiar.org/). The slope was expressed in degrees, while the aspect varied from 1 to 360.

Twenty-seven years (1990, 2000, 2010, and 2013 to 2017), Landsat data were obtained from the United States Geological Survey (USGS) web engine (http://earthexplorer.gov/) (see Table 1). Landsat data were analyzed using SVM, NBT, and KLR algorithms. Their respective training datasets were used to compare the textural features (forests and non-forest regions) and to visually verify the obtained forest maps.

The data processing strategy was divided into two major parts. The first part of the study identified the spatio-temporal distribution of forests, which included the following steps: 1) Download Landsat data from the USGS for the years (1990, 2000, 2010, and 2013 to 2017). All the images had less than 10% cloud cover. 2) For atmospheric correction, we used the Fast Line-of-Sight Atmospheric Analysis of Spectral Hypercubes (FLAASH) module in ENVI v_5.4 [47–50]. FLAASH method consist of radiometric calibration and dark subtraction. Every Digit Number (DN) was transformed into a Top Of Atmosphere (TOA) reflectance through the process of radiometric calibration, beta nought calibration. The calibration type was reflectance, the output interleave was BSQ, the output data type was float, and the scale factor was set to 1 for this TOA calculation. Band minimum conversion of time-averaged optical attenuation (TOA)

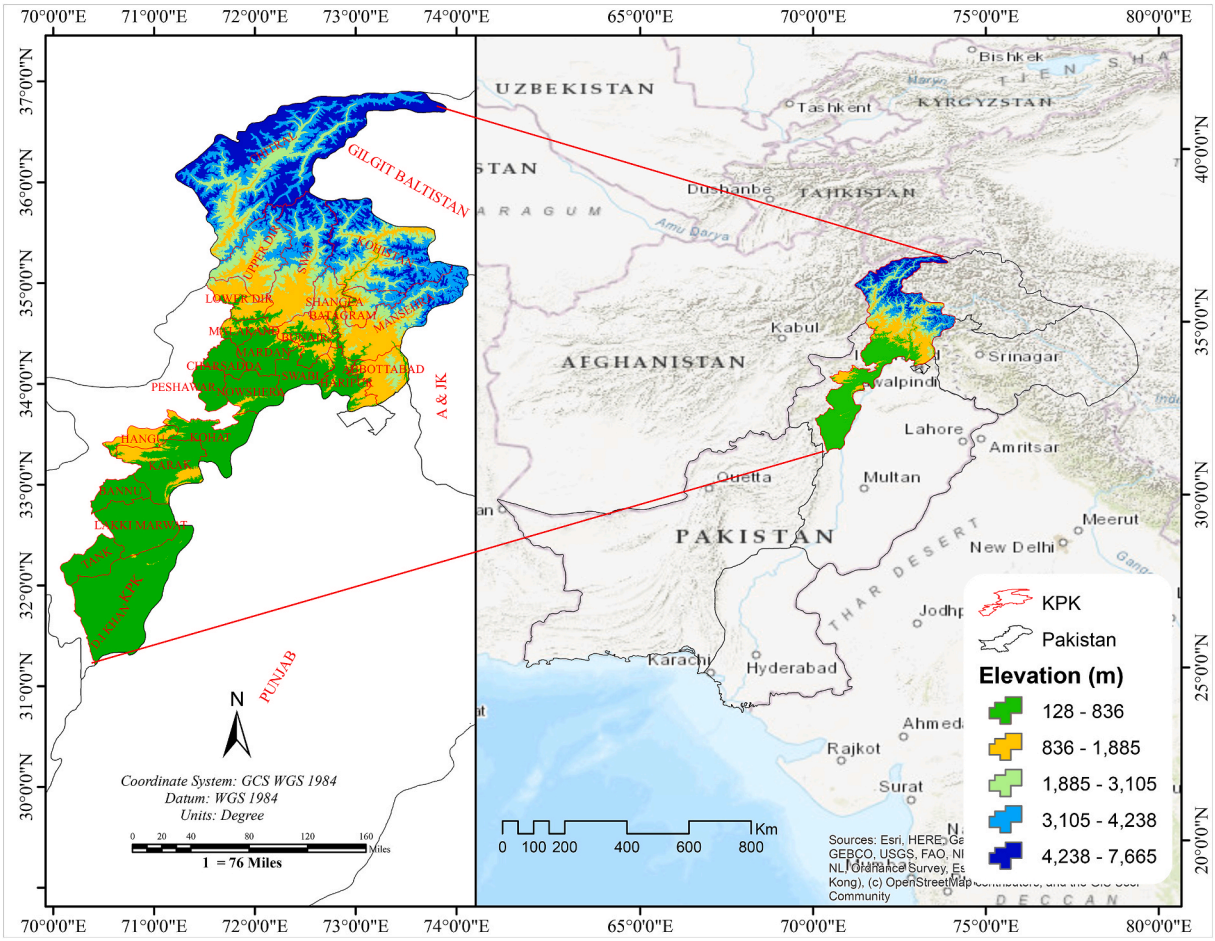


**Fig. 1.** Location of the study area with elevation in meters.

**Table 1**
Datasets were used in the study.

| S. No | Acquisition Date | MOSAIC | | Sensor/Product | Source | Purpose | Processing Level |
|---|---|---|---|---|---|---|---|
| | | Path | Row | | | | |
| 01 | May 1990 | 150 and 151 | 34,35,36,37 and 38 | TM | USGS-EROS | LULC | TIER 1 |
| 02 | May 2000 | 150 and 151 | 34,35,36,37 and 38 | ETM+ | | | |
| 03 | May 2010 | 150 and 151 | 34,35,36,37 and 38 | ETM+ | | | |
| 04 | May 2013 | 150 and 151 | 34,35,36,37 and 38 | OLI/TIRS | | | |
| 05 | May 2014 | 150 and 151 | 34,35,36,37 and 38 | OLI/TIRS | | | |
| 06 | May 2015 | 150 and 151 | 34,35,36,37 and 38 | OLI/TIRS | | | |
| 07 | May 2016 | 150 and 151 | 34,35,36,37 and 38 | OLI/TIRS | | | |
| 08 | May 2017 | 150 and 151 | 34,35,36,37 and 38 | OLI/TIRS | | | |
| 09 | 2018 | | | SRTM | SRTM | Elevation Map | |

to Surface Reflectance (SR) was used in dark object subtraction [51,52]. 3) Layer stacking and mosaicking after atmospheric correction in ERDAS Imagine 2015.4) Subset study area in Arc GIS (Arc Map) 10.8.4) Subset of shapefile in Arc GIS 10.8 using raster calculator. 5) Land cover classification mapping in Erdas imagine 2015.6) Statistical calculation of forest cover change in ENVI v_5.4.7). We used GPS for field survey and comparatively high-resolution Google Earth images for accuracy assessment in ARC GIS 10.8. Finally, we used forest cover mapping and calculation of change detection from 1990 to 2017 in Arc Map 10.8. All methodology was explained in Fig. 2.

### *2.3. Machine learning for image classification*

#### *2.3.1. Support vector machine*

For advanced machine learning tasks, the SVM provides a suite of highly effective algorithms [53]. The goal of SVMs is to design an ideal hyperplane, also known as a decision boundary, which exploits the distance between the nearest samples (support vectors) to the plane and neatly divides classes [54–56]. The model prioritizes training instances that occur at the class distribution's periphery the support vectorswhile effectively discarding the rest [53]. One of the benefits of using the algorithm is that it can achieve high accuracy even with very small training datasets, which helps to reduce the overall cost of training data gathering. The SVM method of classification is based on the assumption that only training samples located on the class boundaries are necessary to make accurate distinctions [55].

The way the training samples are spread out has a big effect on the mathematical definition and design of the optimum hyperplane, i.e. whether the datasets can be separated well or only with some errors. To further regularize/compensate for misclassification/errors, the slack variable I and penalty value (C), also known as cost value, are included in cases of indiscernible samples to punish the outliers. Finally, for purely separable samples, the optimum hyperplane is determined by minimizing the norm (w) function F(w), equation (1);

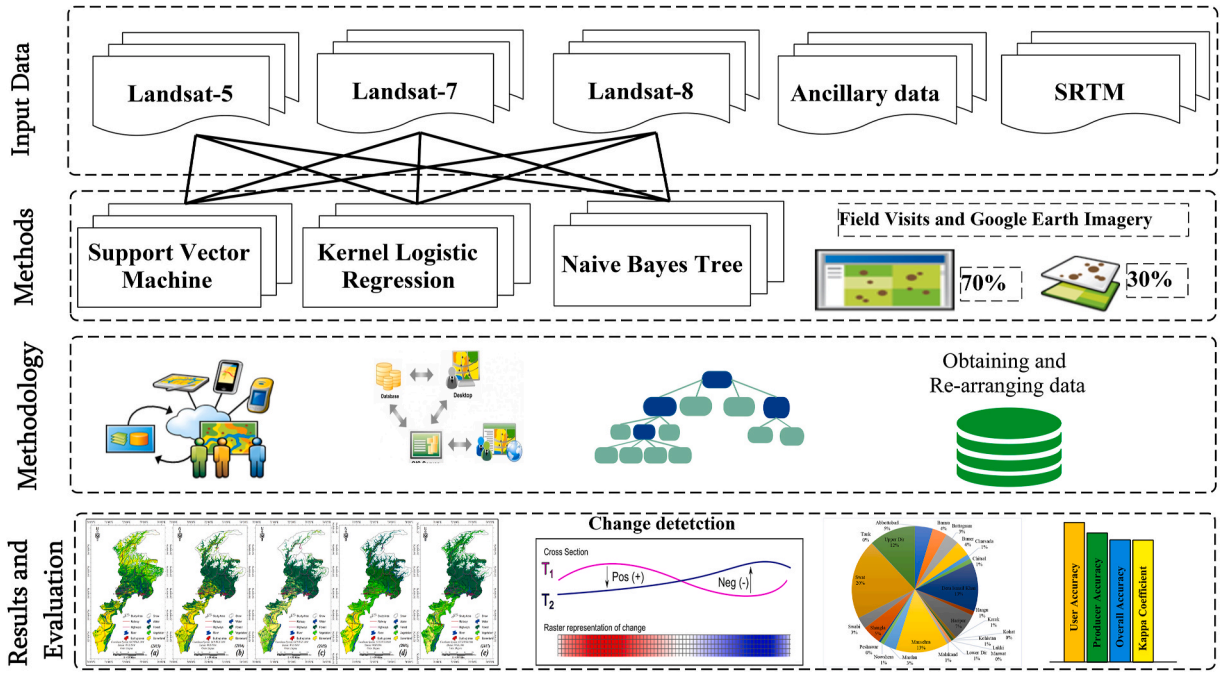


**Fig. 2.** Flow chart explain the methodology of the study (Khyber Pakhtun Khwa Province, Pakistan).

and for F(w), equation (2), for non-differentiable data, which is the most prevalent form of data in remote sensing [55,57] Consequently, we may write them in mathematical notation as [55]:

$$F(W) = (ww)^{1/2} \tag{1}$$

$$F(W, \xi) = (ww)^{1/2} + C\left(\sum_{i=1}^{k} \xi_i\right)^{1} \tag{2}$$

Accuracy and/or generalizability are heavily influenced by misclassified training datasets, in which the data sit on the incorrect side of the ideal hyperplane [55,57], and the variable $C$ is used to mechanism the level of the consequence to regularize such datasets in another function (equation (2)). Overfitting and reduced ability to generalize unknown data result from a high penalty factor, which is achieved by setting $C$ to a large number. Alternatively, if it is too small, it can lead to smoothing, which is the same as having a biased model or underfitting [55,57]. Because of this, it is essential that this parameter be set to the correct value [58]. recommends a middle-of-the-road value in this regard as a means of resolving the tension between the two alternatives [53]. They include the parameters of the kernel functions used to project/map samples that cannot be classified linearly to a higher dimensional space where they can be classed linearly, and the type of kernel functions used to do so [55].

The present study classified twenty-seven-year data collected from Landsat 5, 7, and 8 to calculate the snow, water, barren land, built-up area, forest area, and natural vegetation/shrubs from 1990 to 2017. This study analyzed LULC changes in the 1990–2010 (20 years period) and 2013–2017 (5 years period). The forest area was given due importance as our main objective was to calculate the changes in the forest area that occurred from 1990-to 2017. SVM performed a similar type of analysis, which distinguished homogeneous representative samples of the different kinds of interest on the surface cover. The classification of image data was generated using trained sites, then used to suit the pixels found by the SVM.

### 2.3.2. Kernel logistic regression

Discriminative ML classifier Kernel Logistic Regression (KLR) uses the Broyden-Fletcher-Goldfarb-Shanno (BFGS) optimization technique to produce probabilistic output that is then used to distinguish between the forests and non-forests classes [55]. As its name implies, this kind of logistic regression uses kernel functions to map the input feature space onto a higher-dimensional feature space through following equation (3) [26].

The kernel function is the fundamental function in which φ is assumed that is unknown.

$$K\ (x, x) = \varphi(x)^{T}(x) \tag{3}$$

where $T$ is the inner product in the $Z$ space. Suppose a set of training dataset $\{x_i, y_i\}^{N_{i=1}}$

With $x_i\ \varepsilon\ R^n$ as input parameters with $n$ variables and $N$ data samples. Here, the input parameters are dense forests, dispersed forests and non forests.

$Y_k\ \varepsilon\ \{1, 0\}$ is the related label that indicates forest and non-forests classes. The KLR was applied to built a non-linear decision boundary that may divide the two classes in the feature space based on the following equation (4):

$$p(x) = \frac{e^{y(x)}}{(1 + e^{y(x)})} = \sum_{k}^{Ni=1} \overline{a}_i K\left(x_i, x_j\right) + b \tag{4}$$

where $y(x)$ is the logistic function with values in $[0, 1]$; αi is a vector of dual model parameters, where as b is the intercept; $K(x_i, x_j)$ is the kernel function. For our study, Radial Basis Function (RBF), which is used widely in the literature, was chosen due its flexibility and reliability [59].

### 2.3.3. Naive bayes tree

Machine learning classifier Naive Bayes Tree (NBT) builds a model based on probabilities. Naive Bayes, an application of Bayes's Theorem, makes the system function. The NB bases its framework off on a Decision Tree (DT), with the NBT model being precisely laid out at each branch's terminal node. The NBT has exceptional classification efficiency and precision [60–62].

Class conditional independence refers to the notion that the effect of one attribute value on a particular class is unrelated to the value of any other attribute in the NBT process. Due to the application of the Bayes rule conditionally, NBT allows datasets to be trained in less time. This is because it treats all vectors as though they are independent [63]. equation (5) of the Bayes can be explained as follows:

$$P(A|B) = \frac{P(B|A)P(A)}{P(B)} \tag{5}$$

Where $P(A|B)$ represent the conditional probability of $A$ given $B$; $P(B|A)$ showed the conditional probability of $A$ given $B$. $P(A)$ explained the event probability of $A$. $P(B)$ explained the probability of event $(B)$.

This classifier was selected because it (i) can be trained and classified rapidly, (ii) is resistant to noise in the form of inappropriate landscapes, (iii) is simple to implement and comprehend, and (iv) can be used effectively with very small quantities of training datasets [64].

The model begins with a series of probability estimates for each class, a calculation of the covariance and variance matrix, and the construction of the perception function [65]. Mapping and monitoring of forests in the KLR and NB were conducted using SATISTICA v. 7 [66–68].

Regression issues involving the prediction and mapping of continuing dependent variables are common applications of these tools' stochastic gradient boosting tree [69]. Then, after adjusting the settings, the system was optimized. This includes variables like the number of additive trees, the learning rate, the percentage of subsampling and etc. An ideal learning rate of 0.1 was used, with 185 additive trees and a maximum tree size of 5. Exactness of results may depend on these numbers [70]. The R package was used to carry out the classification process [71].

### 2.4. Ensemble of SVM, KLR and NBT

The stacking approach was used to construct the joint model, and a threshold of 0.9 was applied to identify forest pixels. Models are constructed for the SVM, NBT, and KLR, ML algorithms using the "glmet" R package and the specified training datasets.

### 2.5. Model validation

Forest maps were normalized and compared pixel-by-pixel in order to assess the classifiers' efficacy, with values calculated for forest commission, total incorrect pixels, omission, precession, percentage of incorrect pixels, F1 and recall score. Once classification has been completed, it is crucial to assess classifier efficacy. Precision, accuracy, recall, and the F1 score were all shown to be useful measures of confusion, but the F1 score has gained the most traction in the research [24,72]. Precision, sccuracy, F1 score and recall may all be broken down into its component parts by looking at these four metrics: True Negative (TN), True Positive (TP), False Negative (FN), and False Positive (FP). The following equations 6–10 can be used to determine the precision, accuracy, F1 score and recall:

$$\text{Accuracy} = \text{TP} + \left(\frac{\text{TN}}{\text{TP}}\right)\text{FP} + \text{FN} + \text{TN} \tag{6}$$

$$\text{Kappa} = \text{po} - \frac{\text{pe}}{1} - \text{pe} \tag{7}$$

where $p_o$ is the observed agreement ratio and $p_e$ is the expected agreement

$$\text{Precision} = \frac{\text{TP}}{\text{TP}} + \text{FP} \tag{8}$$

$$\text{Recall} = \frac{\text{TP}}{\text{TP}} + \text{FN} \tag{9}$$

$$\text{F1} = 2 \times \text{precision} \times \frac{\text{recall}}{\text{precision}} + \text{recall} \tag{10}$$

where *TP* denotes a true positive result, *FP* a false positive, and *FN* is the false negative result. Free and open-source R 4.0.0 was used to conduct the performance analysis of the ML algorithms.

### 2.6. Training data collections

Improved classification accuracy can be achieved by using training datasets with higher spatial resolutions, but this can only be achieved by careful attention paid to the training data collecting process [73]. This technique creates training sample sizes that are proportional to the size of the classes by segmenting the population into similar subsets. Because of its proven effectiveness in lowering both bias and error rates, we choose to utilize this technique [53].

The classified images were validated using Google Earth (GE) and GPS points. The random sample point method within the Arc GIS spatial analyst was used to collect random points on the classified land uses of forests and non-forests images. These points were then translated and superimposed on GE into a kml format. Visual interpretation, expert experience and the values of GE points were evaluated. 1114 spatial training samples were obtained from a GPS field survey. The accuracy of classified images was measured using 70% (780)for forestmapping and training and 30% (334) for testing (validation) GPS points. Finally, comparing random samples and GPS with GE images was used to establish the uncertainty matrix. The uncertainty matrix was used to determine the specificity of the SVM land use/cover classification. We have used the Kappa Coefficient (K) as a predictor to confirm the qualitative consensus, either positive or negative, between graded samples and ground-truth points. The relative change of the classifier over ground-truth samples of land-use groups is usually determined from a mathematical evaluation.

### 2.7. Change detection

When comparing two classed images, the ID algorithm finds the difference in their DN values (1990–2000, 2000–2010, 2010–2017,

1990–2017, and 2013–2017). This can be used as a gauge of forest transformation across the KPK. The input parameters for change monitoring are the number of classes, the threshold value, and the type of change detection. Based on the type of remote sensing data, a threshold value is used to determine where in each class the forests have changed [74].

For simple difference, the cutoffs are uniformly distributed between (+1) and (−1). The first (n/2) classes are represented by the negative changes (positive value), and the latter ($n/2$) classes by the positive changes. Normalizing the images (raster maps) by subtracting the image minimum yields the no-change class $[(n/2) + 1]$, which represents the middle class (Fig. 2). Positive changes were shown by red pixels in the final state image of the change detection maps, whereas negative changes were indicated by blue pixels (initial state image). The Envi v.5.4 program included a change detection tool that was used to track the KPK forest as it evolved over time.

## 3. Results

### 3.1. Evaluation of machine learning performance and optimal parameterization

Fig. 3a, b and c compare the accuracy of SVM, KLR, and NBT in terms of recall and F1. The highest F1 scores (0.95) were obtained using SVM and KLR, while the lowest F1 score (0.85) was found with NBT. SVM and KLR algorithms were shown to have slightly different F1 scores. It indicates that the disparity in overall incorrect pixels between SVM, KLR, and NBT is responsible for the disparity in precision and recall scores. When compared to NBT, SVM and KLR shown superior capacity in differentiating between sparse and dense forests. All models, however, had a diminished capacity to identify forests due to their F1 score (0.8), which reflected a decreased capacity to distinguish between isolated forests. This reduced precision is the result of both reduced discrimination ability between forest and non-forest areas and reduced reflectivity inside forest areas. In comparison to NBT's predictions, those made by the SVM and KLR cover a broader range of forest coverage (Fig. 3d). A total of 103,559 km$^2$ was forecast by SVM, whereas 103,129 km$^2$ was forecast by KLR. Nonetheless, the NBT's forecast forest cover is less extensive than what can be seen in Landsat satellite images.

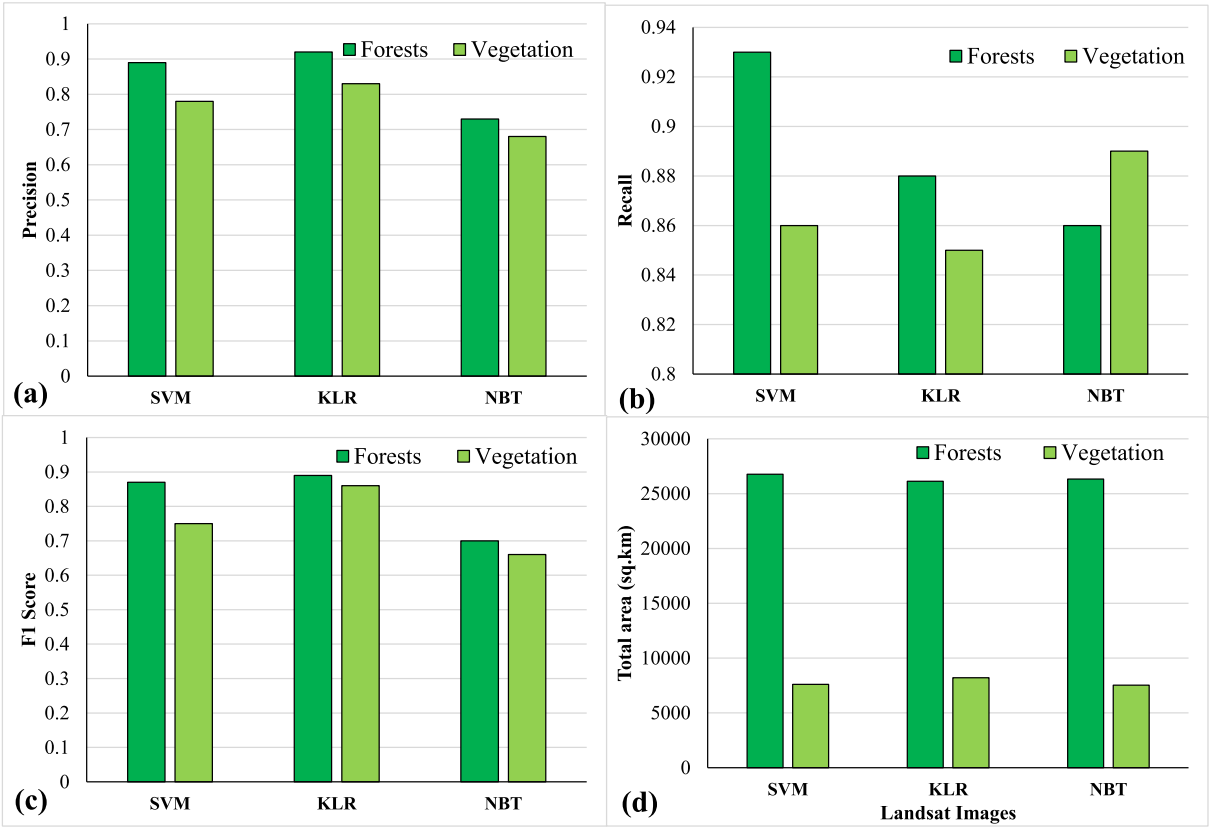


**Fig. 3.** Feature extraction and mapping of the total area (in Km$^2$) from Landsat images of 2017 using SVM, KLR, and NBT models; (a) Precision, (b) Recall, (c) F1 Score, and (d) commulative area.

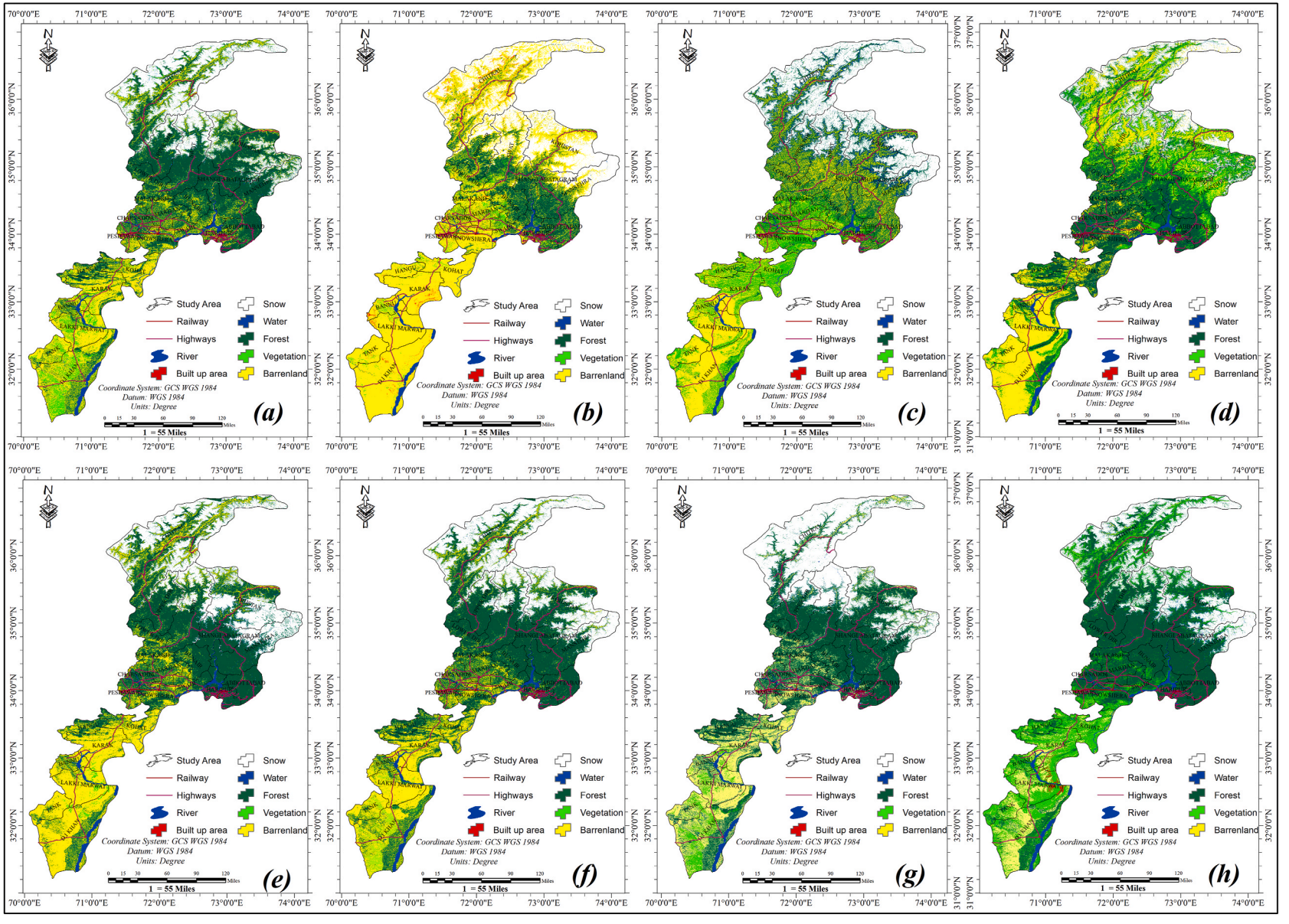


**Fig. 4.** Landuse/cover maps of (a) 1990, (b) 2000, (c) 2010, (d) 2013, (e) 2014, (f) 2015, (g) 2016, (h) 2017).

### 3.2. Landuse landcover classification

Fig. 4(a–h) illustrates the LULC classification obtained from SVM from 1990 to 2017 using Landsat 5, 7, and 8 satellite images. Mostly snow was displayed in northern areas of the KPK (Chitral) region, indicated in blue. Water bodies were displayed in the blue site, mainly in Abbottabad, Peshawar, Upper Dir, and Lower Dir. Indus River and Tarbella dam are primary freshwater sources in KPK. Forest area, barren land, built-up area, and vegetation were displayed in dark green, yellow, red, and light green colors. In all LULC maps from 1990 to 2017, snow areas were seen in most Chitral regions.

### 3.3. Change detection

During 1990 to 2000 forest area was decreased from 19,360 km$^2$ (26.0%) to 19,072 km$^2$ (26.6%), while barren land and built-up area increased from 19,801 km$^2$ (26.6) to 20,113 km$^2$ (27.0%) and 12,134 km$^2$ (16.4) to 12,525 km$^2$ (16.8%) respectively (Fig. 5a). From 2000 to 2010, forest area rapidly decreased due to urbanization and deforestation in KPK province. Forest area and vegetation was decreased 19,072 km$^2$ (25.6%) to 18,784 (25.2%) and 8601 km$^2$ (11.5%) to 8265 km$^2$ (11.1%), while barren land and built-up area was increased from 20,113 km$^2$ (27.0%) to 20,425 km$^2$ (27.4%) displayed in Fig. 5b. Fig. 5c clearly illustrates the forest decrease of almost 576 (almost 1%) of the total forest class of KPK from 2000 to 2010. Table 2 and Fig. 5d present variations in seasonal LULC distribution recorded at high accuracy using the SVM between 1990 and 2017. The accumulation of Forest areas in the central and

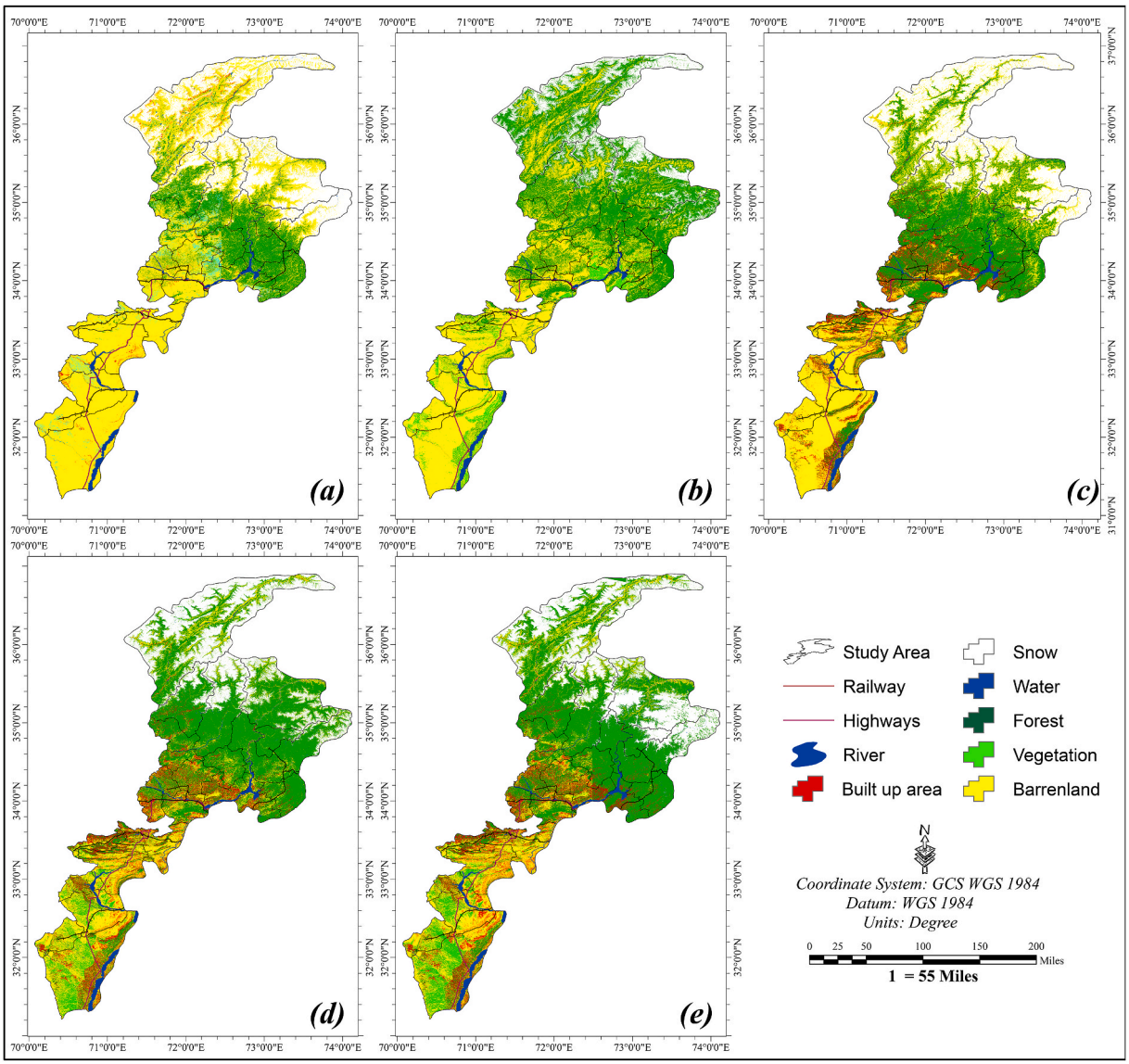


**Fig. 5.** Change detection map from (a) 1990–2000, (b) 2000–2010, (c) 2010–2017, (d) 1990–2017 and (e) 2013–2017.

northern regions is extended from 2013 to 2017. Before this time, the span of forest area was decreased from 1990 to 2010. Table 2 describes, built-up area, water, and vegetation area, Built-up area and forest area was increased from 12,213 $km^2$ (16.4%) to 13,173 $km^2$ (17.7%), 3041 $km^2$ (4.1%) to 3515 $km^2$ (4.7%) and 8937 $km^2$ (12%) to 9177 $km^2$ (12.3%) (Table 2). Meanwhile, snow, barren land and forest class decreased from 11,169 $km^2$ (15%) to 10,695 $km^2$ (14.4%), 19,801 $km^2$ (26.6%) to 19,321 $km^2$ (25.9%) and 19,360 $km^2$ (26.0%) to 18,640 $km^2$ (25%) respectively (Table 2). In the end, Fig. 5e displays the 2013 to 2017 forest class results. 2013–2017 showed that the area of forest cover increased from 18,640 $km^2$ (25.0) to 26,765 $km^2$ (35%) due to the one billion tree project. The change was 3.61 % as compared to the year 2015–2016. The overall change was 8.74 % forest area was increased from 2013-to 2017.

Forest cover was changed yearly to 25.39%, 27.23%, 30.52%, 34.13% for 2013, 2014, 2015, 2016, and 2017 respectively. Overall forest cover area from 2013 to 2017 was changed by 30–46% of the total area of the study region. The results of forest cover change as calculated by change detection have been shown in Fig. 5. The overall result of forest cover in 2013–2014 was 37,836 $km^2$ area covered with forest, and 111,206 $km^2$ area was shown non-forest of the total area of KPK. The change was 3.61 % as compared to the year 2015–2016. In 2014 and 2015, the forest-covered area was 40,578 $km^{2,}$ and 108,464 $km^2$ area was non-forest covered. In 2015–2016, the forest-covered area was 45,483 $km^{2,}$ and 103,559 $km^2$ was non-forest covered. Only 3 .29% of forest-covered were increased during 2015–2016.

## 4. Discussion

The study investigated the numerous land cover types in KPK Province in Pakistan. The classified results more administered the changes that had fallen between the identified classes.

### 4.1. Evaluation of the performance of the classifiers

Accurate forest mapping, classification, and 27 years change monitoring across ecosystems were made possible through the application and performance comparison of SVM, NBT and KLR, algorithms. SVM achieved the highest levels of accuracy, recall, and F1 score of any machine learning technique. Consequently, the SVM has a robust capacity to map forests across a variety of habitats. According to these findings, the SVM and KLR can identify dense forest sections that stand in for the entire forest. When compared to other methods, NBT's F1 score was the lowest (0.8), indicating its poorer forest detection performance (Fig. 4).

The F1 scores of SVM iterations were 0.93 and 0.90, respectively, whereas those of KLR iterations were 0.90 and 0.89. These results agreed well with other research that has found the SVM algorithm to be more accurate than the CART [75], RF [76], and maximum likelihood [77], who evaluated the efficacy of groundwater aid using machine learning methods to that of classical classifiers.

The results are consistent with those of [78]; who tested several classifiers for change monitoring and found that the SVM, which makes use of publicly available Landsat imagery, was the most effective. From multiple time-series of high-resolution remote-sensing images [79], implemented a change detection method using visual saliency and SVM. When it came to mapping forests, however, conventional classifiers actually had the opposite effect.

When compared to ML classifiers that used commercially accessible remote sensing data like LiDAR and WorldView-3, the accuracy of using publicly available Landsat images to recognize forests was on par [78,79]. SVM's total accuracy only reached 82%, despite the excellent spatial resolution of the LiDAR, WorldView, and Rapid Eye images [75]. In LULC classification, other investigations verified that the Rotation of Forest (RoF) approach, which is less sensitive than the SVM algorithm, was more accurate than the Canonical Correlation Forest (CCF) [34,75].

The suggested method significantly improves the efficiency of both linear and non-linear classifiers and constitutes a departure from traditional forests classes and LULC. With proper tuning, ML algorithms can improve classification quality and robustness [80, 81]. Processing massive volumes of remote sensing data quickly and cheaply was made possible by the widespread availability and simple implementation of ML, as well as the free availability of Landsat images [78,79].

### 4.2. Re-forestration of change detection

Our findings indicate that Landsat data combined with an SVM classification technique allows the LULC to be highly OA. Relevant satellite data is essential for achieving high accuracy levels. Despite a comparatively higher resolution, Landsat data is constrained not

**Table 2**
LULC from 1990 to 2017.

| Class Name | Area in $Km^2$ (Percentage) | | | | | | | |
|---|---|---|---|---|---|---|---|---|
| | 1990 | 2000 | 2010 | 2013 | 2014 | 2015 | 2016 | 2017 |
| Snow | 11,169 (15.0) | 11,122 (14.9) | 10,652 (14.3) | 10,695 (14.4) | 9962 (13.4) | 10,627 (14.3) | 8850 (11.9) | 8703 (11.7) |
| Water | 3041 (4.1) | 3088 (4.1) | 3558 (4.8) | 3515 (4.7) | 3598 (4.8) | 2116 (2.8) | 3254 (4.4) | 2932 (3.9) |
| Barren Land | 19,801 (26.6) | 20,113 (27.0) | 20,425 (27.4) | 19,321 (25.9) | 18,491 (24.8) | 16,137 (21.7) | 15,204 (20.4) | 14,377 (19.3) |
| Built up area | 12,213 (16.4) | 12,525 (16.8) | 12,837 (17.2) | 13,173 (17.7) | 13,480 (18.1) | 13,730 18.4 | 13,974 (18.8) | 14,134 (19.0) |
| Forest area | 19,360 (26.0) | 19,072 (25.6) | 18,784 (25.2) | 18,640 (25.0) | 19,196 (25.8) | 21,382 (28.7) | 24,101 (32.3) | 26,765 (35.9) |
| Vegetation | 8937 (12.0) | 8601 (11.5) | 8265 (11.1) | 9177 (12.3) | 9794 (13.1) | 10,529 (14.1) | 9138 (12.3) | 7610 (10.2) |

to promptly collect geospatial data, limiting its suitability for flood monitoring and mapping [82,83]. However, two Landsat satellite paths (150 and 151) enabled the acquisition of high-temporal resolution Landsat data (16 days) in the study area, compared to a single temporal resolution of 15 days for the site [84]. Cloud cover presence will restrict the availability of images of flood instances. Compared to optical satellites, SAR (Sentinel 1,2,3) and RADAR satellites can quickly penetrate clouds and acquire images (Landsat, MODIS) [82]. Variations that occurred during the period 2013-14 showed that forests had increased by 2.98%. From 2014 to 2015, the forest was the only prevailing land cover, with an area of 19,196 $km^2$ 2014. However, it was enlarged to 21,382 $km^2$ in 2015 (Fig. 6).

The subsequent prevalent land cover in terms of terrestrial size was barren land that ensured a size reduction in 2015, but in 2014 it became the most dominant land cover with a total size of 18,491 $km^2$. The increase in the forest over the period confirmed the report by Bhaduri [85]. Change detection for 2014 to 2015 showed that forest area increased by 11.39%, making almost 2186 $km^2$. In this period, the forest-covered area was 27.23% of the total area of the study region. Almost 2719 $km^2$ of the new area was included in the forest class, almost 12.72% [86]. In this period, the forest-covered area was 30.52% of the total area of the study region. During the period 2016–17, the forest was the only most prevalent land cover, with an area of 24,101 $km^2$ in 2016. It had improved to 26,765 $km^2$ in 2017. But in 2016, it emerged as the most dominant land cover, with an overall area of 15,204 $km^2$ [87]. Forest area was increased to 11.05%, making almost 2664 $km^2$. In this period, the forest-covered area was 34.13% of the total area of the study region (Fig. 6).

The forest cover change map for 2013, 2014, 2015, 2016, and 2017 are shown in Fig. 6, respectively. For the year 2013, the map indicates that only a few districts of KPK were covered with forest, and a deficient proportion of forest cover was observed. During 2014, an increase in forest cover area was observed, although less. In 2015, the Government of Kpk made policies to improve the forest cover area and control deforestation. During 2016 and 2017, a significant increase in forest cover area was observed, likely due to the initiative of the tsunami of billion tree project in KPK province [42].

In this analysis, various products, sensors, and algorithms were compared to show the uncertainty of estimating forests. Based on the fact that there was an increase in the forest area, this paper suggested using different methods to secure forest areas. We developed a new way for reforestation and forest monitoring for the "One Billion Tree Project" plan in KPK, Pakistan. According this period, 2013–2017, almost 8125 $km^2$ area was included in the forest class [42].

The long-term Landsat-based forest maps generated in this research provide accurate and updated estimates of forest cover in KPK, Pakistan. Our findings, however, only illustrate the general dynamics of forest cover without details on forest composition, tree height, or the average age of observed forests. Optical sensors, including canopy closing and density, are more susceptible to horizontal tree structures. Vertical structure parameters are difficult to obtain or extract using only the visible spectral bands of Landsat images. On the other hand, appropriate field investigation samples are necessary to identify low and high-density forests or young and mature forests. However, in KPK, Pakistan, we have minimal field samples with these attributes. The combination of optical and microwave data and the GEE application now provides an excellent opportunity to obtain exact forest maps on a regional or global scale. For better estimates of forest areas and their transitions, image fusion and robust classification algorithms should be considered a priority.

Furthermore, owing to the "One Billion Tree" schemes in KPK, Pakistan, our analysis demonstrated a slight net loss of forests and some afforestation. However, proper identification of forest quality or the reaction of vegetation to changing climate and human activity is rarely recorded in this area. Future studies should focus on better and more accurate databases to have credible policy-making knowledge eventually to explore these issues.

## 5. Conclusions

This research proposed a unified strategy for integrating SVM learning with high-resolution spatial training data, SVM optimal parameterization, and post-classification improvement of the resulting forests and non-forests maps. Sample node value of 7, tree depth value of 0, and tree in forest value of 75 were found to be optimal settings. The results showed that the integration strategy, which makes use of Landsat imagery, is able to distinguish between forest and non-forest regions, with an increased overall accuracy of 6.7% compared to supervised classifications. The findings also revealed that KPK woods had expanded everywhere throughout the course of the last 27 years.

One of the approaches had been used successfully using multispectral and multi-temporal satellite imagery with a resolution of 30 m. It was observed that the imagery should be captured in middle infrared and near-infrared bands of the spectrum for high detection rates. Furthermore, the current study proved that vegetation and snow effectively determine forest cover change. Our findings, forest area, vegetation and snow area was decreased from 19,360 $km^2$ (26.0%) to 18,784 (25.2%), 8937 $km^2$ (12.0%) to 8,601 $km^2$ (11.5%), and 11,169 $km^2$ (15.0%) to 10,652 $km^2$ (14.3%), while barren land built-up area and water area was increased from 19,801 $km^2$ (26.6%) to 20,113 $km^2$ (27.0%), 12,213 $km^2$ (16.4%) to 12,525 $km^2$ (16.8%), and 3041 $km^2$ (4.1%) to 3558 $km^2$ (4.8%) in 1990–2010. Forest class rapidly increased due to one billion projects from 18,640 $km^2$ (25.0%) to 26,765 $km^2$ (35.9%), increasing almost 8125 $km^2$ from 2013 to 2017.

Further study will be conducted using multi-temporal Landsat data from 1990 to 2017 for identification of the spatio-temporal distribution of forest cover area according to forest type and using Cellular Automata Markov Chain analysis for future prediction of forest cover change. The study demonstrated concurrent reforestation in barren land areas. It has improved the methods to sustain the forest and RS and GIS in everyday forestry organization practices in the KPK area. This research would be highly effective, especially at the decision-making level.

## Author contribution statement

Aqil Tariq: Conceived and designed the experiments; Performed the experiments; Analyzed and interpreted the data; Contributed

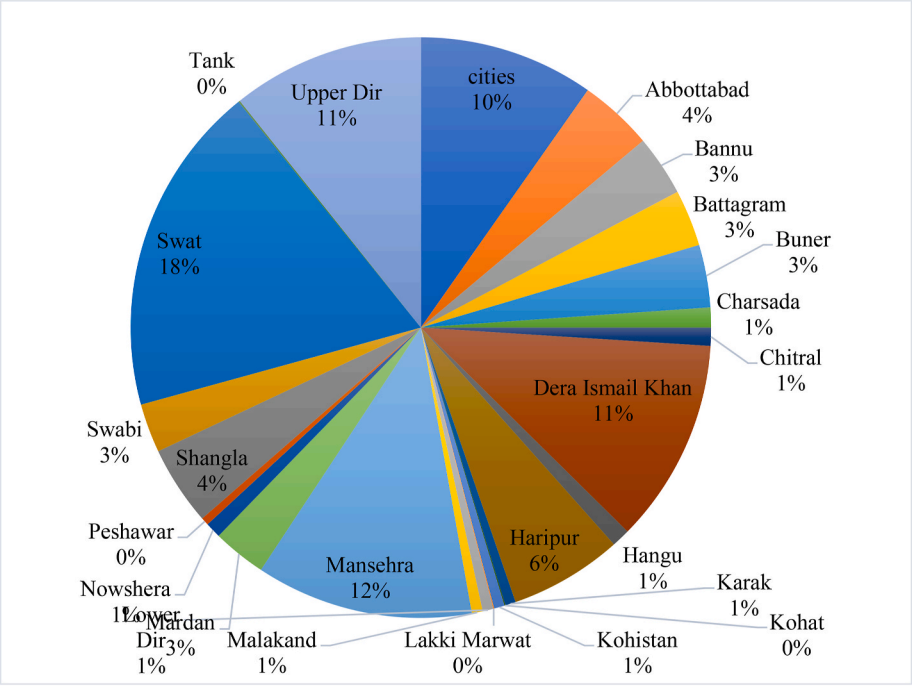


**Fig. 6.** Re-forestation map from 2013 to 2017.

reagents, materials, analysis tools or data; Wrote the paper. Yan Jiango, Qingting Li, Jianwei Gao, Walid Soufan, Khalid F. Almutairi, Muhammad Habib-ur-Rahman and Linlin Lu; Contributed reagents, materials, analysis tools or data; Wrote the paper.

## Funding statement

This work is supported by the National Natural Science Foundation of China (grant nos. 41901292 and 42071321). The authors extend their appreciation to Researchers Supporting Project number (RSPD2023R561), King Saud University, Riyadh, Saudi Arabia.

## Data availability statement

Data included in article/supp. Material/referenced the in article.

## Declaration of interest's statement

The authors declare that they have no known competing financial interests or personal relationships that could have appeared to influence the work reported in this paper.

## Acknowledgments

The authors extend their appreciation to Researchers Supporting Project number (RSPD2023R561), King Saud University, Riyadh, Saudi Arabia. We would like to pay special thanks to USGS (Earth explorer) department for providing us Landsat and MODIS data. The authors would like to thanks Sumaira Jamil for her enthusiastic support and valuable suggestions during the manuscript review. The authors thank for the valuable comments of the both reviewers and editors and their promising suggestions to improve this paper.

## References

[1] A.S. Mather, The forest transition, Area 24 (4) (1992) 367–379. Available at: https://www.scopus.com/inward/record.uri?eid=2-s2.0-0026959543&partnerID=40&md5=9fd31d9f04f81e478687c630884b461f.
[2] K.A. Oduro, et al., Tracing forest resource development in Ghana through forest transition pathways, Land Use Pol. 48 (2015) 63–72, https://doi.org/10.1016/j.landusepol.2015.05.020.
[3] M.S. Park, Y.C. Youn, Reforestation policy integration by the multiple sectors toward forest transition in the Republic of Korea, For. Pol. Econ. 76 (2017) 45–55, https://doi.org/10.1016/j.forpol.2016.05.019.
[4] E. Hendrick, K. Black, Climate Change and Irish Forestry, COFORD Connects, 2009, p. 9.
[5] A. Tariq, J. Yan, B. Ghaffar, et al., Flash flood susceptibility assessment and zonation by integrating analytic hierarchy process and frequency ratio model with diverse spatial data, Water 14 (19) (2022) 3069, https://doi.org/10.3390/w14193069.

[6] A. Tariq, et al., Spatio-temporal assessment of land use land cover based on trajectories and cellular automata Markov modelling and its impact on land surface temperature of Lahore district Pakistan, Environ. Monit. Assess. 195 (1) (2023) 114, https://doi.org/10.1007/s10661-022-10738-w.
[7] A. Tariq, J. Yan, F. Mumtaz, Land change modeler and CA-Markov chain analysis for land use land cover change using satellite data of Peshawar, Pakistan, Phys. Chem. Earth, Parts A/B/C 128 (89) (2022), 103286, https://doi.org/10.1016/j.pce.2022.103286.
[8] D. Brack, Forests and Climate Change Duncan Brack I the Fourteenth Session of the United Nations Forum on Forests, 2019.
[9] P.H. Verburg, et al., Analysis of the effects of land use change on protected areas in the Philippines, Appl. Geogr. 26 (2) (2006) 153–173, https://doi.org/10.1016/j.apgeog.2005.11.005.
[10] P. Coppin, et al., Digital change detection methods in ecosystem monitoring: a review, Int. J. Rem. Sens. 25 (9) (2004) 1565–1596, https://doi.org/10.1080/0143116031000101675.
[11] R.K. Ningthoujam, et al., Mapping forest cover and forest cover change with airborne S-band radar, Rem. Sens. 8 (7) (2016), https://doi.org/10.3390/rs8070577.
[12] A. Sajjad, et al., Application of Remote Sensing and GIS in Forest Cover Change in Tehsil Barawal (June), 2015, pp. 1501–1508.
[13] T. Report, Mitigating climate variability and change Farmers, in: C.M. Davis, B. Bernart, Dmitriev A. Corvallis (Eds.), Strategies for Adapting to and Mitigating Climate Variability and Change through Agroforestry in Ethiopia and Kenya', *Forestry Communications Group*, Oregon: Oregon State University, 2015 (February).
[14] A. Tariq, H. Shu, A.S. Gagnon, et al., Assessing burned areas in wildfires and prescribed fires with spectral indices and SAR images in the margalla hills of Pakistan, Forests 12 (10) (2021) 18, https://doi.org/10.3390/f12101371.
[15] A. Tariq, H. Shu, S. Siddiqui, I. Munir, et al., Spatio-temporal analysis of forest fire events in the Margalla Hills, Islamabad, Pakistan using socio-economic and environmental variable data with machine learning methods, J. For. Res. 13 (2021) 12, https://doi.org/10.1007/s11676-021-01354-4.
[16] A. Tariq, F. Mumtaz, et al., Spatio-temporal Variation of Seasonal Heat Islands Mapping of Pakistan during 2000–2019, Using Day-Time and Night-Time Land Surface Temperatures MODIS and Meteorological Stations Data, Remote Sensing Applications: Society and Environment, 2022, 100779, https://doi.org/10.1016/j.rsase.2022.100779.
[17] L. Hasan, Analysing Institutional Set-Up of Forest Management in Pakistan, 2008. Available at: https://mpra.ub.uni-muenchen.de/7343/.
[18] T. Ali, B. Shahbaz, A. Suleri, Analysis of myths and realities of deforestation in northwest Pakistan: implications for forestry extension, Int. J. Agric. Biol. 8 (1) (2006) 1560–8530. Available at: http://www.fspublishers.org.
[19] I.R. Ejiagha, et al., Urban warming of the two most populated cities in the Canadian province of alberta, and its influencing factors, Sensors 22 (8) (2022), https://doi.org/10.3390/s22082894.
[20] C. Hong, et al., Global and regional drivers of land-use emissions in 1961–2017, Nature 589 (7843) (2021) 554–561, https://doi.org/10.1038/s41586-020-03138-y.
[21] E. Kalnay, M. Cai, Impact of urbanization and land-use, Nature 425 (6939) (2003) 528–531, https://doi.org/10.1038/nature01649.1.
[22] S. Mansour, et al., Forecasting of built-up land expansion in a desert urban environment, Rem. Sens. 14 (9) (2022), https://doi.org/10.3390/rs14092037.
[23] M. Rahman, et al., Flooding and its relationship with land cover change, population growth, and road density, Geosci. Front. 12 (6) (2021), 101224, https://doi.org/10.1016/j.gsf.2021.101224.
[24] X.P. Song, et al., Global land change from 1982 to 2016, Nature 560 (7720) (2018) 639–643, https://doi.org/10.1038/s41586-018-0411-9.
[25] H. Yohannes, et al., Impact of landscape pattern changes on hydrological ecosystem services in the Beressa watershed of the Blue Nile Basin in Ethiopia, Sci. Total Environ. 793 (2021), 148559, https://doi.org/10.1016/j.scitotenv.2021.148559.
[26] H. Yohannes, et al., Spatio-temporal changes in habitat quality and linkage with landscape characteristics in the Beressa watershed, Blue Nile basin of Ethiopian highlands, J. Environ. Manag. 281 (June 2020) (2021), 111885, https://doi.org/10.1016/j.jenvman.2020.111885.
[27] F. Mumtaz, et al., Modeling spatio-temporal land transformation and its associated impacts on land surface temperature (LST), Rem. Sens. 12 (18) (2020), https://doi.org/10.3390/RS12182987.
[28] B. Matsushita, et al., Sensitivity of the enhanced vegetation index (EVI) and normalized difference vegetation index (NDVI) to topographic effects: a case study in high-density cypress forest, Sensors 7 (11) (2007) 2636–2651, https://doi.org/10.3390/s7112636.
[29] A. Tariq, I. Riaz, Z. Ahmad, Land surface temperature relation with normalized satellite indices for the estimation of spatio-temporal trends in temperature among various land use land cover classes of an arid Potohar region using Landsat data, Environ. Earth Sci. 79 (1) (2020) 1–15, https://doi.org/10.1007/s12665-019-8766-2.
[30] D. Xu, Compare NDVI extracted from Landsat 8 imagery with that from Landsat 7 imagery, Am. J. Rem. Sens. 2 (2) (2014) 10, https://doi.org/10.11648/j.ajrs.20140202.11.
[31] Z. Jiang, et al., Development of a two-band enhanced vegetation index without a blue band, Rem. Sens. Environ. 112 (10) (2008) 3833–3845, https://doi.org/10.1016/j.rse.2008.06.006.
[32] M. Hasanlou, N. Mostofi, Investigating urban heat island effects and relation between various land cover indices in tehran city using Landsat 8 imagery, in: Proceedings of the 1st International Electronic Conference on Remote Sensing, Basel, Switzerland, 2015, pp. 1–11, https://doi.org/10.3390/ecrs-1-f004.
[33] C. Pelletier, et al., Assessing the robustness of Random Forests to map land cover with high resolution satellite image time series over large areas, Rem. Sens. Environ. 187 (2016) 156–168, https://doi.org/10.1016/j.rse.2016.10.010.
[34] A. Ahmad, et al., A synthesis of spatial forest assessment studies using remote sensing data and techniques in Pakistan, Forests 12 (9) (2021) 1211, https://doi.org/10.3390/f12091211.
[35] A. Tariq, H. Shu, S. Siddiqui, B.G. Mousa, et al., Forest fire monitoring using spatial-statistical and Geo-spatial analysis of factors determining forest fire in Margalla Hills, Islamabad, Pakistan, Geomatics, Nat. Hazards Risk 12 (1) (2021) 1212–1233, https://doi.org/10.1080/19475705.2021.1920477.
[36] F. Zellweger, et al., Disentangling the effects of climate, topography, soil and vegetation on stand-scale species richness in temperate forests, For. Ecol. Manag. 349 (2015) 36–44, https://doi.org/10.1016/j.foreco.2015.04.008.
[37] M.N. Siddiqui, Z. Jamil, J. Afsar, Monitoring changes in riverine forests of Sindh-Pakistan using remote sensing and GIS techniques, Adv. Space Res. 33 (3) (2004) 333–337, https://doi.org/10.1016/S0273-1177(03)00469-1.
[38] M. Aslam, et al., Adaptive machine learning based distributed denial-of-services attacks detection and mitigation system for SDN-enabled IoT, Sensors 22 (7) (2022) 2697, https://doi.org/10.3390/s22072697.
[39] M. Avand, et al., DEM resolution effects on machine learning performance for flood probability mapping, J. Hydro-Environ. Res. 40 (2022) 1–16, https://doi.org/10.1016/j.jher.2021.10.002.
[40] S. Felegari, et al., Integration of sentinel 1 and sentinel 2 satellite images for crop mapping, Appl. Sci. 11 (21) (2021), 10104, https://doi.org/10.3390/app112110104.
[41] D. Tien Bui, H. Van Le, N.D. Hoang, GIS-based spatial prediction of tropical forest fire danger using a new hybrid machine learning method, Ecol. Inf. 48 (August) (2018) 104–116, https://doi.org/10.1016/j.ecoinf.2018.08.008.
[42] R. Hutt, Pakistan Has Planted over a Billion Trees, World Econimic Forum, 2018. Available at: https://www.weforum.org/agenda/2018/07/pakistan-s-billion-tree-tsunami-is-astonishing/.
[43] A.J. Afridi, et al., Land topography and feasibility of an elevated- excavated fish Pond a technical version Khyber, J. Entomol. Zool. Stud. 5 (1) (2017) 113–116.
[44] M.A. Malik, M. Azam, A. Saboor, Water Quality Status of Upper Kpk and Northern Areas of pakistan, 2010.
[45] M. Gašparović, T. Jogun, The effect of fusing Sentinel-2 bands on land-cover classification, Int. J. Rem. Sens. 39 (3) (2018) 822–841, https://doi.org/10.1080/01431161.2017.1392640.
[46] D.P. Roy, et al., Landsat-8: Science and product vision for terrestrial global change research, Rem. Sens. Environ. 145 (2014) 154–172, https://doi.org/10.1016/j.rse.2014.02.001.
[47] R. Avtar, et al., Exploring renewable energy resources using remote sensing and GIS—a review, Resouces 8 (149) (2019) 23.
[48] L.S. Bernstein, et al., Validation of the QUick atmospheric correction (QUAC) algorithm for VNIR-SWIR multi- and hyperspectral imagery, in: Algorithms and Technologies for Multispectral, Hyperspectral, and Ultraspectral Imagery XI, 5806(March 2018), 2005, p. 668, https://doi.org/10.1117/12.603359.

[49] R. Richter, R. Applications, Atmospheric/Topographic Correction for Satellite Imagery, Wessling, Germany, 2016.
[50] U.S. Environmental Protection Agency, Quality Assurance Guidance Document 2.12, 2016. Available at: https://www3.epa.gov/ttnamti1/files/ambient/pm25/qa/m212.pdf.
[51] J.J. Erinjery, M. Singh, R. Kent, Mapping and assessment of vegetation types in the tropical rainforests of the Western Ghats using multispectral Sentinel-2 and SAR Sentinel-1 satellite imagery, Rem. Sens. Environ. 216 (July) (2018) 345–354, https://doi.org/10.1016/j.rse.2018.07.006.
[52] Z. Shao, L. Zhang, Estimating forest aboveground biomass by combining optical and SAR data: a case study in genhe, inner Mongolia, China, Sensors 16 (6) (2016), https://doi.org/10.3390/s16060834.
[53] A. Tariq, J. Yan, A.S. Gagnon, et al., Mapping of cropland, cropping patterns and crop types by combining optical remote sensing images with decision tree classifier and random forest, Geo Spatial Inf. Sci. (2022) 1–19, https://doi.org/10.1080/10095020.2022.2100287, 00(00).
[54] C. Cortes, V. Vapnik, Support-vector networks, Mach. Learn. 20 (3) (1995) 273–297, https://doi.org/10.1007/bf00994018.
[55] C. Huang, L.S. Davis, J.R.G. Townshend, An assessment of support vector machines for land cover classification, Int. J. Rem. Sens. 23 (4) (2002) 725–749, https://doi.org/10.1080/01431160110040323.
[56] S. Hussain, et al., Spatiotemporal variation in land use land cover in the response to local climate change using multispectral remote sensing data, Land 11 (5) (2022) 595, https://doi.org/10.3390/land11050595.
[57] G.M. Foody, A. Mathur, A relative evaluation of multiclass image classification by support vector machines, IEEE Trans. Geosci. Rem. Sens. 42 (6) (2004) 1335–1343, https://doi.org/10.1109/TGRS.2004.827257.
[58] X. Yang, Parameterizing support vector machines for land cover classification, Photogramm. Eng. Rem. Sens. 77 (1) (2011) 27–37.
[59] S. Das, Geospatial mapping of flood susceptibility and hydro-geomorphic response to the floods in Ulhas basin, India, Remote Sens. Appl.: Society and Environment 14 (2019) 60–74, https://doi.org/10.1016/J.RSASE.2019.02.006.
[60] M.J. Aitkenhead, et al., Estimating soil properties from smartphone imagery in Ethiopia, Comput. Electron. Agric. 171 (February) (2020), 105322, https://doi.org/10.1016/j.compag.2020.105322.
[61] S. Felegari, A. Sharifi, K. Moravej, Investigation of the relationship bet een NDVI inde , soil moisture , and precipitation data using satellite images, in: Sustainability, 2022, p. 12.
[62] M. Majeed, et al., A detailed ecological exploration of the distribution patterns of wild poaceae from the jhelum district (Punjab), Pakistan, Sustainability 14 (7) (2022) 3786, https://doi.org/10.3390/su14073786.
[63] S.S. Wahla, et al., Assessing spatio-temporal mapping and monitoring of climatic variability using SPEI and RF machine learning models, Geocarto Int. (2022) 1–20, https://doi.org/10.1080/10106049.2022.2093411, 0(0).
[64] B. Pradhan, et al., Soil erosion assessment and its correlation with landslide events using remote sensing data and GIS: a case study at Penang Island, Malaysia, Environ. Monit. Assess. 184 (2) (2012) 715–727, https://doi.org/10.1007/s10661-011-1996-8.
[65] J. Hooker, G. Duveiller, A. Cescatti, Data descriptor: a global dataset of air temperature derived from satellite remote sensing and weather stations, Sci. Data 5 (2018) 1–11, https://doi.org/10.1038/sdata.2018.246.
[66] A. Sowter, et al., Mexico City land subsidence in 2014–2015 with Sentinel-1 IW TOPS: results using the Intermittent SBAS (ISBAS) technique, Int. J. Appl. Earth Obs. Geoinf. 52 (2016) 230–242, https://doi.org/10.1016/j.jag.2016.06.015.
[67] A. Tariq, H. Shu, S. Siddiqui, M. Imran, et al., Monitoring land use and land cover changes using geospatial techniques, A case study of fateh jang, attock, Pakistan, Geogr. Environ. Sustain. 14 (1) (2021) 41–52, https://doi.org/10.24057/2071-9388-2020-117.
[68] J. Yang, Y.Q. Zhao, J.C.W. Chan, Hyperspectral and multispectral image fusion via deep two-branches convolutional neural network, Rem. Sens. 10 (5) (2018), https://doi.org/10.3390/rs10050800.
[69] O. Satir, S. Berberoglu, A. Cilek, Modelling long term forest fire risk using fire weather index under climate change in Turkey, Appl. Ecol. Environ. Res. 14 (4) (2016) 537–551, https://doi.org/10.15666/aeer/1404_537551.
[70] Y. Chen, et al., Mapping croplands, cropping patterns, and crop types using MODIS time-series data, Int. J. Appl. Earth Obs. Geoinf. 69 (March) (2018) 133–147, https://doi.org/10.1016/j.jag.2018.03.005.
[71] A.J. Arnfield, Two decades of urban climate research: a review of turbulence, exchanges of energy and water, and the urban heat island, Int. J. Climatol. 23 (1) (2003) 1–26, https://doi.org/10.1002/joc.859.
[72] R. Firdaus, N. Nakagoshi, A. Idris, Sustainability assessment of humid tropical watershed: a case of batang merao watershed, Indonesia, Procedia Environ. Sci. 20 (2014) 722–731, https://doi.org/10.1016/j.proenv.2014.03.086.
[73] C.H. Key, N.C. Benson, Landscape Assessment (LA) Sampling and Analysis Methods, USDA Forest Service - General Technical Report RMRS-GTR, 2006 (164 RMRS-GTR).
[74] A. Tariq, H. Shu, CA-Markov chain analysis of seasonal land surface temperature and land use landcover change using optical multi-temporal satellite data of Faisalabad, Pakistan, Rem. Sens. 12 (20) (2020) 1–23, https://doi.org/10.3390/rs12203402.
[75] D. Somasundaram, et al., Learning vector quantization neural network for surface water extraction from Landsat OLI images, J. Appl. Remote Sens. 14 (3) (2020) 1, https://doi.org/10.1117/1.jrs.14.032605.
[76] Global Forest Observations Initiative, Integrating Remote-Sensing and Ground-Based Observations for Estimation of Emissions and Removals of Greenhouse Gases in Forests, 2014.
[77] M. Won, K. Kim, S. Lee, Analysis of burn severity in large-fire area using SPOT5 images and field survey data, Korean J. Agric. For. Meteorol. 16 (2) (2014) 114–124, https://doi.org/10.5532/KJAFM.2014.16.2.114.
[78] Q. Weng, Thermal infrared remote sensing for urban climate and environmental studies: methods, applications, and trends, ISPRS J. Photogrammetry Remote Sens. 64 (4) (2009) 335–344, https://doi.org/10.1016/j.isprsjprs.2009.03.007.
[79] A. Pang, M.W.L. Chang, Y. Chen, Evaluation of random forests (RF) for regional and local-scale wheat yield prediction in southeast Australia, Sensors 22 (3) (2022) 1–19, https://doi.org/10.3390/s22030717.
[80] S. Abdullahi, B. Pradhan, Land use change modeling and the effect of compact city paradigms: integration of GIS-based cellular automata and weights-of-evidence techniques, Environ. Earth Sci. 77 (6) (2018) 1–15, https://doi.org/10.1007/s12665-018-7429-z.
[81] S.R. Morshed, M.A. Fattah, Responses of spatiotemporal vegetative land cover to meteorological changes in Bangladesh, Remote Sens. Appl.: Society and Environment 24 (March) (2021), 100658, https://doi.org/10.1016/j.rsase.2021.100658.
[82] Z.N. Musa, I. Popescu, A. Mynett, A review of applications of satellite SAR, optical, altimetry and DEM data for surface water modelling, mapping and parameter estimation, Hydrol. Earth Syst. Sci. 19 (9) (2015) 3755–3769, https://doi.org/10.5194/hess-19-3755-2015.
[83] S. Qi, et al., Inundation extent and flood frequency mapping using LANDSAT imagery and digital elevation models, GIScience Remote Sens. 46 (1) (2009) 101–127, https://doi.org/10.2747/1548-1603.46.1.101.
[84] B. Khalid, et al., Riverine flood assessment in Jhang district in connection with ENSO and summer monsoon rainfall over Upper Indus Basin for 2010, Nat. Hazards 92 (2) (2018) 971–993, https://doi.org/10.1007/s11069-018-3234-y.
[85] A. Bhaduri, Climate change, Econ. Lab. Relat. Rev. 23 (3) (2012) 3–12, https://doi.org/10.1177/103530461202300301.
[86] A. Raziq, A. Xu, Y. Li, Monitoring of land use/land cover changes and urban sprawl in peshawar city in khyber pakhtunkhwa: an application of geo- information techniques using of multi-temporal satellite data, J. Remote Sens. GIS 5 (4) (2016), https://doi.org/10.4172/2469-4134.1000174.
[87] Z. Lu, et al., The effect of forest tenure on forest composition in a miao area of guizhou, China, Mt. Res. Dev. 36 (2) (2016) 193–202, https://doi.org/10.1659/mrd-journal-d-15-00057.1.